

Article

Microstructure and Dielectric Properties of LPCVD/CVI-SiBCN Ceramics Annealed at Different Temperatures

Jianping Li ¹, Mingxi Zhao ¹, Yongsheng Liu ^{1,2,*}, Nan Chai ¹, Fang Ye ¹, Hailong Qin ¹, Laifei Cheng ¹ and Litong Zhang ¹

- ¹ Science and Technology on Thermostructural Composite Materials Laboratory, Northwestern Polytechnical University, Xi'an 710072, China; ijianping@163.com (J.L.); mingxizhao@mail.nwpu.edu.cn (M.Z.); chainan.90@163.com (N.C.); yefang511@nwpu.edu.cn (F.Y.); qinxlong555@163.com (H.Q.); chenglf@nwpu.edu.cn (L.C.); zhanglt@nwpu.edu.cn (L.Z.)
- ² State Key Laboratory of Solidification Processing, Northwestern Polytechnical University, Xi'an 710072, China
- * Correspondence: yongshengliu@nwpu.edu.cn or liuys99067@163.com; Tel.: +86-29-8849-5179; Fax: +86-29-8849-4620

Academic Editor: Jérôme Chevalier

Received: 5 April 2017; Accepted: 7 June 2017; Published: 15 June 2017

Abstract: SiBCN ceramics were introduced into porous Si₃N₄ ceramics via a low-pressure chemical vapor deposition and infiltration (LPCVD/CVI) technique, and then the composite ceramics were heat-treated from 1400 °C to 1700 °C in a N₂ atmosphere. The effects of annealing temperatures on microstructure, phase evolution, dielectric properties of SiBCN ceramics were investigated. The results revealed that α-Si₃N₄ and free carbon were separated below 1700 °C, and then SiC grains formed in the SiBCN ceramic matrix after annealing at 1700 °C through a phase-reaction between free carbon and α-Si₃N₄. The average dielectric loss of composites increased from 0 to 0.03 due to the formation of dispersive SiC grains and the increase of grain boundaries.

Keywords: siliconboron carbonitride ceramic; dielectric properties; electromagnetic wave absorbing properties; heat treatment; chemical vapor deposition and infiltration

1. Introduction

Siliconboron carbonitride ceramics (SiBCN) are considered as promising materials for high-temperature structural ceramics, continuous fiber reinforced ceramic matrix composites (CFCC) [1–5], and agents for electromagnetic wave (EMW) absorber [6], etc., because of their low density, supreme ultra-high temperature stability up to 2000 °C [7], good resistance to oxidation and creep [8], and high strength and modulus [7–9]. More importantly, with the development of stealth, radar-absorbing technology, and telecommunications, the study of EMW absorption has gained worldwide interest [10–12]. For non-magnetic ceramic materials, ideal EMW absorption materials must satisfy two requirements: (1) the impedance matching between free space and the material surface to prevent the wave being reflected, which requires the complex permittivity to be close to 1; and (2) materials can absorb as many incident waves as possible inside of absorbers, which requires materials exhibit strong dielectric loss [13]. In the quaternary SiBCN ceramics, SiC is a wide band gap semiconductor material and carbon is a good conductor, both of which have excellent EMW absorption and shielding properties and can be good dielectric loss phases [12,14,15]. Si₃N₄ and BN have low dielectric constants and dielectric losses, which can be regarded as wave-transparent matrices and impedance matching phases. Therefore, SiBCN ceramics have aroused much enthusiasm for high-temperature functional materials not only because of the excellent EMW absorption property

but also due to the controllable EMW absorption property by designing phase composition and microstructure [16,17].

Recently, many methods have been developed to prepare different types of SiBCN ceramics, including the polymer pyrolyzing route [18], chemical vapor deposition and infiltration (CVD/CVI) [19,20], reactive magnetron sputtering [21], and a mechanical alloying plus sintering technique [22]. EMW-absorbing properties of SiBCN ceramics made by polymer pyrolyzing and CVD/CVI was studied. Ye et al. [16] fabricated SiBCN ceramics with extremely low dielectric loss (about 0.01) via polymer-derived ceramics (PDCs), while their dielectric property is improved significantly when annealed above 1650 °C owing to the crystallization of SiC grains and structural transformation. The element content and phase composition of ceramics fabricated via PDCs can be adjusted by controlling the structure of the precursor. Wang et al. [23] found that β -Si₃N₄ and β -SiC were separated when a novel SiBCN ceramic was annealed at 2200 °C in N₂ atmosphere. Therefore, the structural transformation of SiBCN ceramics after annealing at high temperature may have a positive impact on their dielectric and EMW absorbing capabilities.

In our previous work, low-pressure chemical vapor deposition/infiltration (LPCVD/CVI) SiBCN ceramics, which have been designed by thermodynamic calculation, have various and complex phases, such as Si₃N₄+SiC+C+BN, SiC+C+B and B₄C+SiC+C+BN, when using a gas mixture of CH₃SiCl₃-NH₃-BCl₃-H₂ and the phase content can be controlled by adjusting experimental conditions [20]. In our previous researches, LPCVD/CVI technology was used for the first time to introduce SiBCN ceramics into porous Si₃N₄ substrates [24]. The obtained SiBCN ceramic was amorphous and SiBCN-Si₃N₄ composite ceramics had a dielectric loss of 0 when fabricated at 800 °C and 0.1 at 900 °C, exhibiting tunable EMW absorbing capability [24].

Generally, high temperature has an important effect on microstructure, phase composition, and properties of ceramic materials. On the one hand, heat treatment is frequently used as the process to improve the functional properties of ceramic materials [16,25]; on the other hand, the microstructure and properties of ceramics might change when used in high-temperature fields. Therefore, it is necessary to investigate the microstructure evolution and impact of separated phases on the dielectric and EMW absorption properties of LPCVD/CVI SiBCN ceramics. Focusing on this purpose, in the present work, the LPCVD/CVI SiBCN ceramics were prepared on a porous Si₃N₄ matrix at 800 °C with the same deposition parameters as those in our previous study [24], and then these composite ceramics were annealed at high temperatures in a nitrogen atmosphere. The thermodynamic diagram demonstrated the SiBCN consisted of Si₃N₄+SiC+C+BN [24]. The effect of the annealing temperature on the microstructure, phase evolution, thermal stability, dielectric, and EMW absorption properties were investigated.

2. Materials and Methods

Si₃N₄ ceramics with porosity of about 30% were used as deposition substrates. The Si₃N₄ ceramics fabricated using the previous method [26] were machined into specimens with dimensions of 2.16 mm × 10.16 mm × 22.86 mm for dielectric properties measurement. Then these samples were put into a CVD/CVI furnace to infiltrate SiBCN ceramics using methyltrichlorosilane (CH₃SiCl₃, MTS ≥ 99.99%), boron trichloride (BCl₃ ≥ 99.99%), and ammonia (NH₃ ≥ 99.99%) as gas resources at 800 °C. The as-received composites were termed as AS. Hydrogen (H₂ ≥ 99.99%) was used as the carrier gas of MTS and the dilution gas. Argon (Ar ≥ 99.9%) was also used as the dilution gas. Finally, these samples were heat-treated at 1400, 1500, 1600, and 1700 °C in a high-purity N₂ atmosphere for 2 h (N₂, 0.3 MPa) using a hot-pressing furnace (High-Multi 5000, Fujidempa Kogyo, Osaka, Japan), and the obtained composite ceramics were named HT-14, HT-15, HT-16, and HT-17, respectively.

Weight loss of SiBCN-Si₃N₄ composite ceramics after annealing was measured by an electronic balance (Mettler Toledo, AG204) with precision of 0.0001 g. The microstructure and phase composition were analyzed by scanning electron microscopy (SEM; S-4700; Hitachi, Tokyo, Japan) and X-ray diffraction (XRD; D8-Advance, Bruker, Karlsruhe, Germany), respectively. X-ray photoelectron

spectrometry (XPS, K-Alpha; Thermo Scientific, Waltham, MA, USA) was carried out to verify the bonding structure. Raman spectra were recorded on a Renishaw Ramoscope (confocal Raman microscope, inVia, Renishaw, Gloucestershire, UK) equipped with a He-Ne laser ($\lambda = 514.5$ nm). The complex permittivity for X-band was measured via a vector network analyzer (VNA, MS4644A; Anritsu, Atsugi, Japan) using the waveguide method.

3. Results and Discussion

As shown in Figure 1, the weight loss of SiBCN-Si₃N₄ composite ceramics increased slightly as the annealing temperature increased. However, a remarkable weight loss of 2.72% was found when the annealing temperature reached 1700 °C, which indicated that there were some reactions occurred, and this may lead to structure transformation or decomposition of SiBCN ceramics. It will be confirmed by our following analysis. The surface morphologies of as-received and annealed SiBCN-Si₃N₄ composite ceramics at different temperatures ranging from 1400 °C to 1700 °C are presented in Figure 2. As we can see from Figure 2a, the as-received SiBCN ceramics via LPCVD/CVI were amorphous with a compact and continuous cauliflower-like surface morphology. However, due to the mismatch in thermal expansion coefficients between SiBCN and Si₃N₄, a large amount of cracks appeared uniformly on the SiBCN coating for all annealed samples. When the temperature was up to 1600 °C, some particles formed in ceramics, which might be attributed to the crystallization of ceramics, and this will be proved by several methods in the following part of the paper. With the further increase of temperature to 1700 °C, more particles and flocculent products covered the surface of SiBCN-Si₃N₄ ceramics. The various surface morphologies at different temperatures indicated that the process of crystallization was strongly influenced by the increase of annealing temperature.

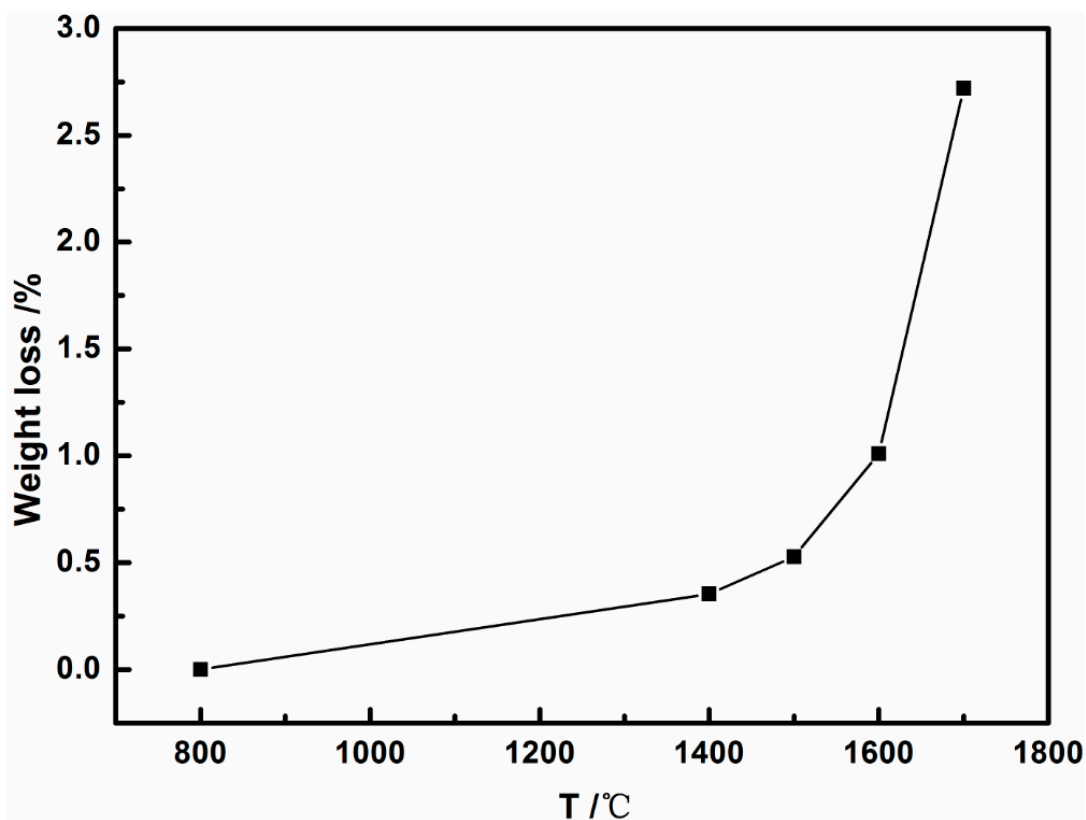


Figure 1. Weight loss of SiBCN-Si₃N₄ composite ceramics after annealing at different temperatures.

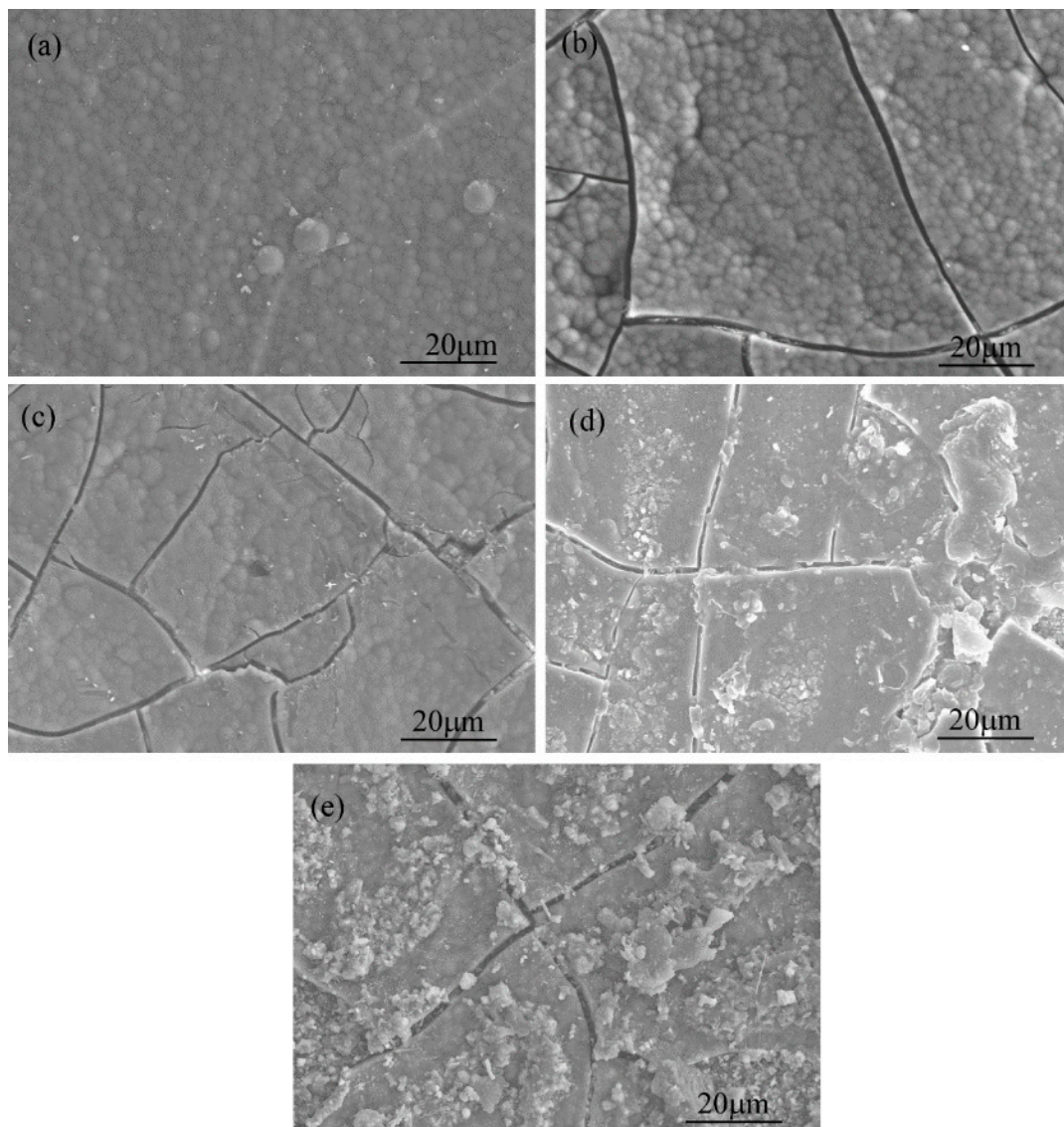


Figure 2. The surface morphology of as-received (a) and annealed SiBCN-Si₃N₄ ceramics at different temperatures: (b) HT-14; (c) HT-15; (d) HT-16; and (e) HT-17.

The Raman spectroscopy technique, with high sensitivity to carbon, was performed to record the structure evolution of free carbon within SiBCN ceramics before and after annealing from 1400 °C to 1700 °C. As shown in Figure 3, there were no bands observed from the spectra of as-received SiBCN ceramic in the whole frequency region, suggesting extremely low free carbon content. After annealing at 1400 °C, two broad signals centered around 1350 cm⁻¹ and 1582 cm⁻¹ appeared and maintained existence to 1600 °C, which were representative features of the free carbon termed D band and G band, respectively. The D and G bands can vary in intensity, position, and width depending on the structural organization of the samples. The intensity ratio of the D and G modes (I(D)/I(G)) can predict the ordering and carbon cluster size of free carbon. The I(D)/I(G) of HT-14, HT-15, and HT-16 were 1.27, 1.27, and 1.19, respectively, implying the free carbon underwent the conversion from amorphous to nanocrystalline graphite when the temperature increased to 1600 °C, according to the three-stage model reported by Ferrari and Robertson [11,27,28]. When the temperature further increased to 1700 °C, there were no D and G bands, which may indicate that the free carbon was consumed to an extremely low content by chemical reactions occurring in the SiBCN ceramic when annealed at 1700 °C. This was confirmed by the following XRD and XPS analysis.

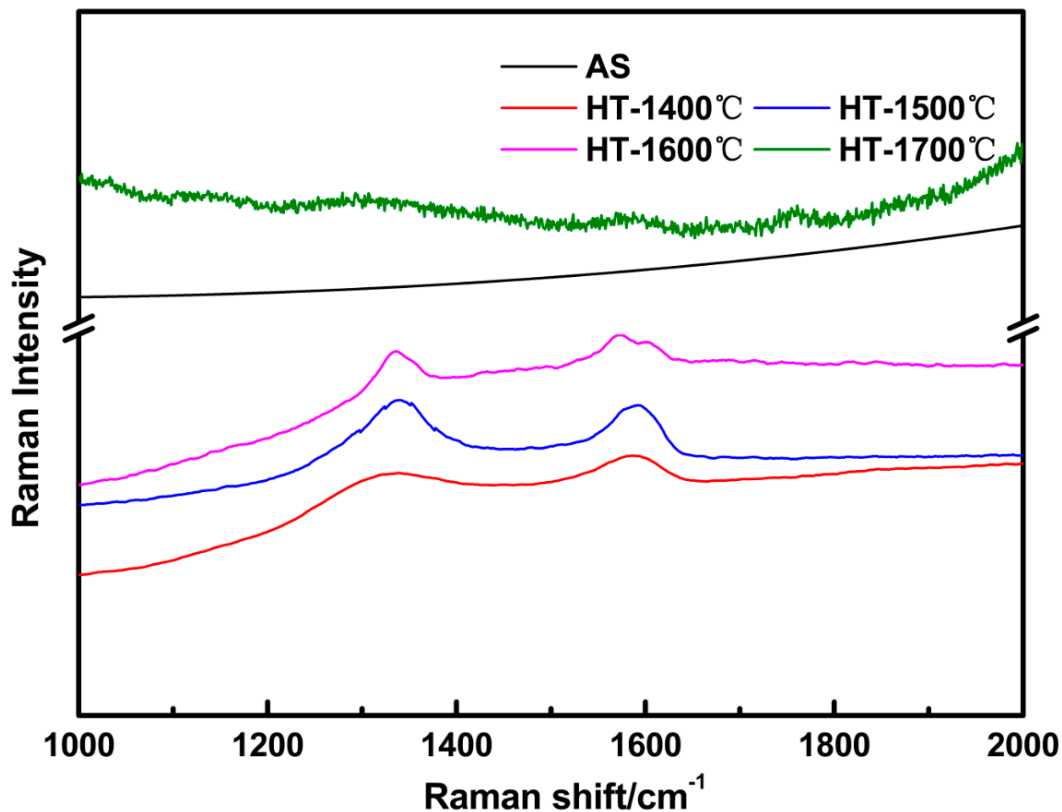
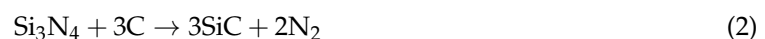


Figure 3. Raman spectra of as-received and annealed SiBCN-Si₃N₄ ceramics at different temperatures.

The crystallization behavior of SiBCN-Si₃N₄ composite ceramics was studied through X-ray diffraction (Figure 4). The spectra of as-received SiBCN ceramic was the same with that of Si₃N₄ substrate which consists of β-Si₃N₄, indicating the amorphous state of as-received SiBCN ceramics. When the temperature increased from 1500 °C to 1700 °C, there were β-SiC peaks in annealed SiBCN and the intensity increased with the increasing temperature. However, the case for α-Si₃N₄ and BN is quite different. The characteristic peaks of α-Si₃N₄ appeared after annealing at 1600 °C, which suggested the crystallization of α-Si₃N₄ occurred. Whereas some of characteristic peaks of α-Si₃N₄ disappeared and the intensity of some decreased after annealing at 1700 °C, indicating the dropped amount of α-Si₃N₄. Additionally, BN showed the same trend that it crystallized at 1600 °C and disappeared at 1700 °C. Therefore, on the basis of XRD and Raman results, it can be concluded that the crystallization phases were Si₃N₄+SiC+C+BN and were consistent with the thermodynamic diagram [24]. Nevertheless, B₄C was found in SiBCN ceramic when annealing at 1700 °C, coupled with decreased intensity of α-Si₃N₄ and disappearances of carbon peaks in Raman spectra, which might indicate that chemical reactions occurred in SiBCN ceramic when annealed at 1700 °C.

In terms of the above results, it can be inferred that chemical reaction occurred in SiBCN ceramic when annealed at 1700 °C, and it was expressed as the following equations:



XPS analysis was carried out to confirm the phase evolution and phase-reaction of SiBCN ceramics annealed at high temperatures. Figure 5 shows the narrow scanning spectra of C1s, B1s, and Si2p of SiBCN film before and after heat treatment. The correction of the XPS spectra was performed using C1s peak ($E_B = 284.6$ eV). For as-received SiBCN, the B1s spectrum was divided into two spectra, i.e., B-N at 191.1 eV and B-O at 193 eV [29]. The C1s peak was fitted into four peaks which

were C-Si around 283.4 eV, free carbon at 284.6 eV, and C-O at 286.0 eV [30]. The relative content of C-C bonds was much higher than that of C-Si bonds, which was in reasonable agreement of the separation of amorphous carbon at 1400 °C. The Si2p peak could be decomposed into two sub peaks centered at 101.4 eV–102.0 eV and 100.4 eV, which should be assigned to Si-N [30] and Si-C [31] bonds, respectively. B-O and C-O bonds vanished simultaneously after annealing at 1600 °C, which confirmed that the slight weight loss of SiBCN-Si₃N₄ composite ceramics annealed before 1600 °C came from the absorption of the impurities in air. After further annealing at 1700 °C, the B-C bonds appeared though its relative content was much lower than B-N bonds, while the C-C bonds disappeared completely, only C-Si bonds remained. The bonds evolution agreed well with the results of XRD and Raman spectra, providing a certain evidence for phase evolution and the occurrence of phase-reaction.

The relative complex permittivity ($\epsilon_r = \epsilon' - j\epsilon''$) was measured in the frequency range of 8.2–12.4 GHz. According to the Debye theory, the real part of permittivity (ϵ') is related to the polarization relaxation and the imaginary part of permittivity (ϵ'') represents the dielectric loss capability [15]. In addition, in order to fabricate the non-magnetic materials with excellent microwave absorption properties, the dielectric constant (real part of the permittivity) should be close to 1, and the dielectric loss (conductivity or imaginary part of the permittivity) should be high enough. Thereby, the dielectric loss ($\tan\delta = \epsilon''/\epsilon'$) can represent the EMW attenuation capacity of non-magnetic materials. This means that higher $\tan\delta$ results in better microwave attenuation capability.

As shown in Figure 6, the complex permittivity of as-fabricated Si₃N₄ substrates was 4.4-j0 and stayed a constant after annealing at 1400–1700 °C due to the unchanged phases and microstructures. The Si₃N₄ substrates were exact insulators, so the complex permittivity of SiBCN-Si₃N₄ composite ceramics was determined mostly by the deposited SiBCN. The average ϵ' and ϵ'' of AS were 4.74 and 0.02, respectively, and the dielectric loss was 0. That was in accordance with the results in our previous work [24] that the SiBCN fabricated at 800 °C was insulating due to the complete amorphous microstructure. After annealing at 1400–1700 °C, there was a slight variation in the average ϵ' . As for the average ϵ'' , it kept a relatively stable value of around 0 after annealing at 1400–1600 °C while exhibiting an increase to 0.15 with the temperature rising to 1700 °C, and the dielectric loss accordingly increased to 0.03.

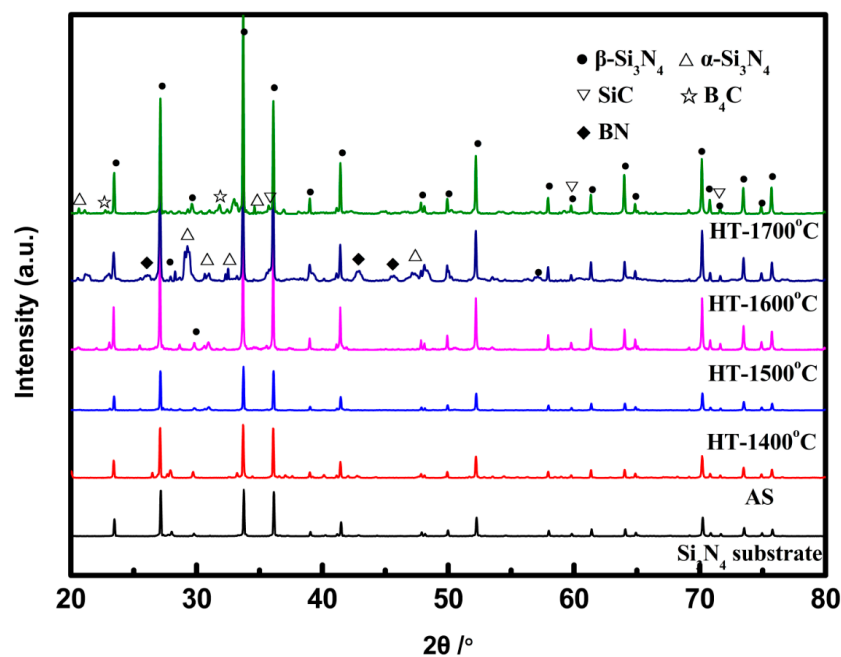


Figure 4. X-ray diffraction patterns of SiBCN-Si₃N₄ ceramics with different heat-treatment temperatures.

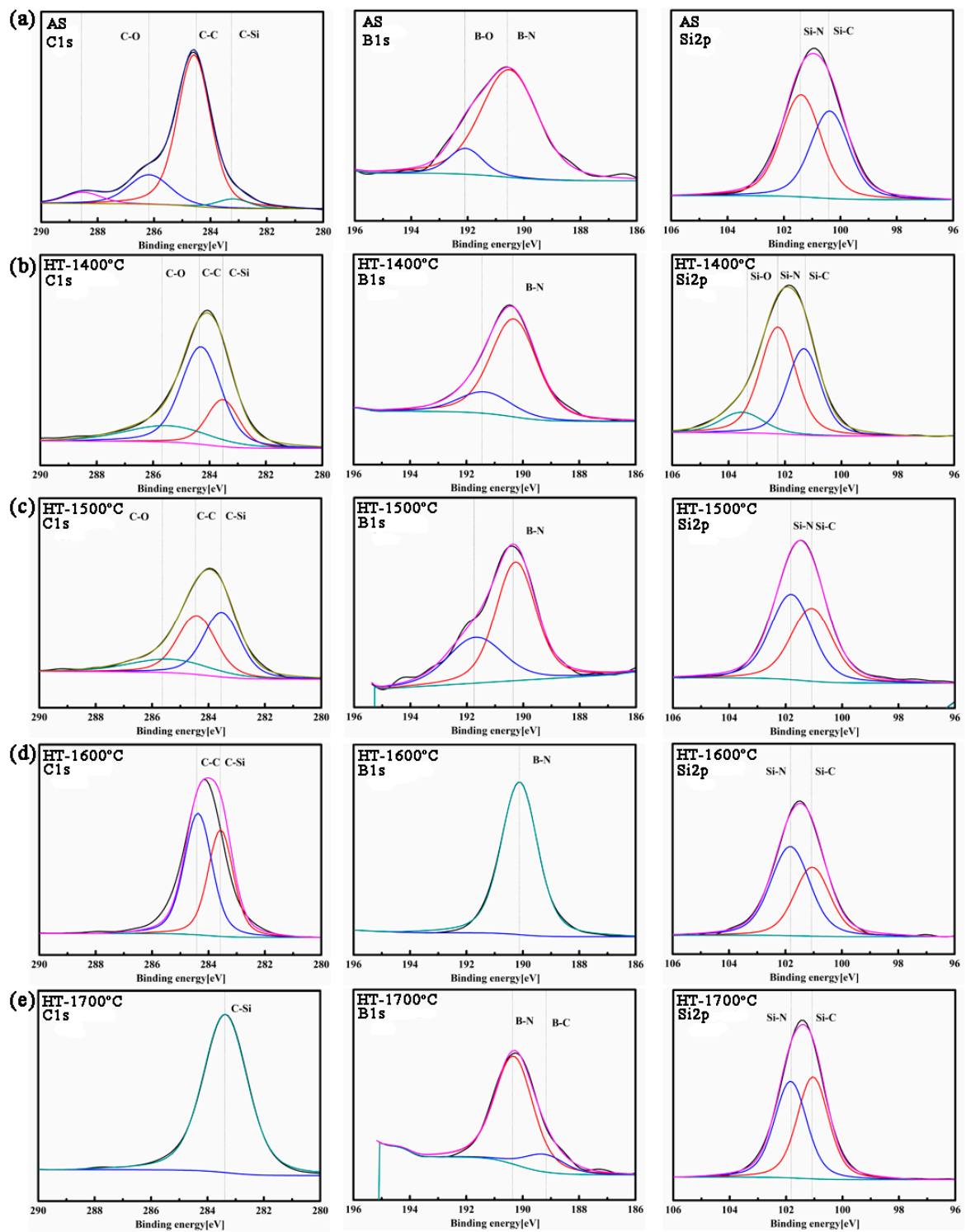


Figure 5. High-resolution XPS spectra of C1s, B1s, and Si2p core levels of SiBCN ceramics: (a) AS; (b) HT-14; (c) HT-15; (d) HT-16; and (e) HT-17.

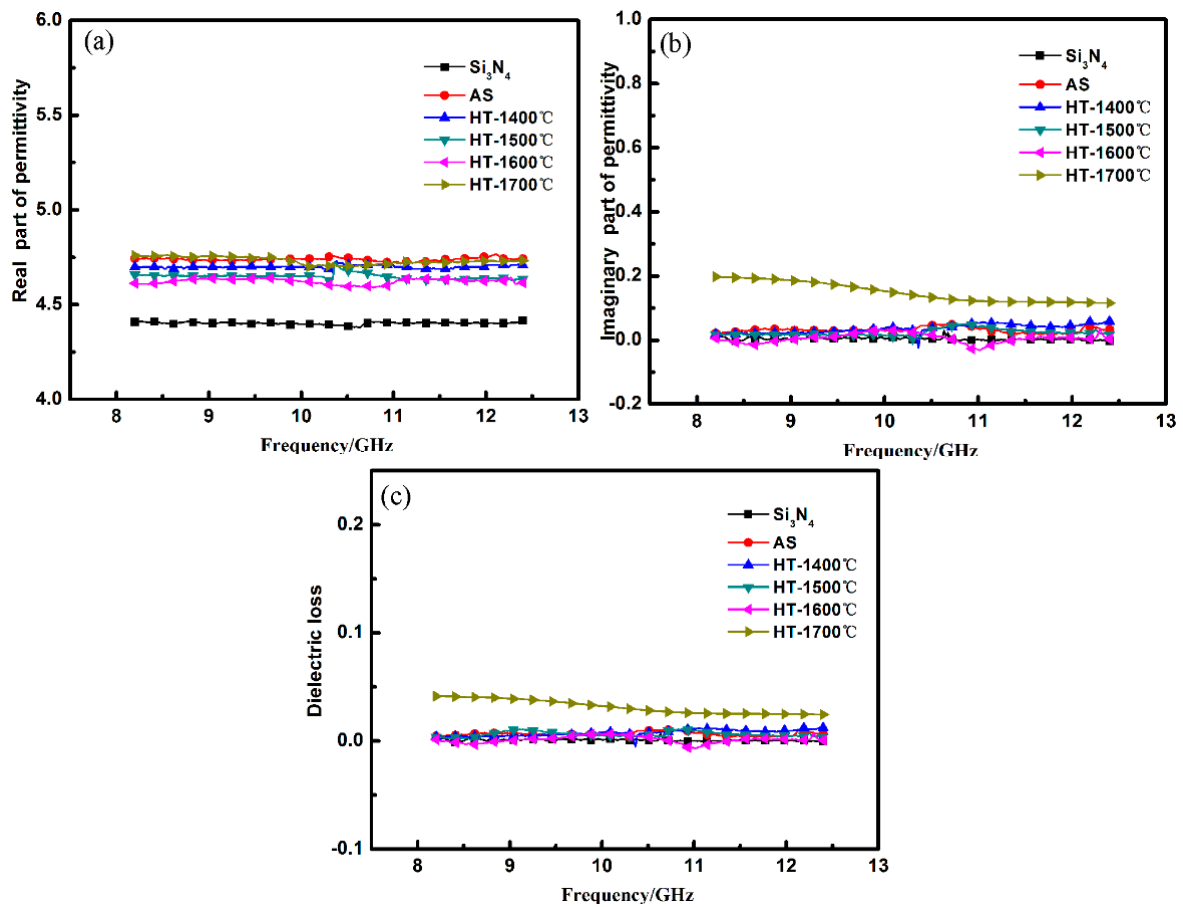


Figure 6. The permittivity of as-received and annealed SiBCN-Si₃N₄ ceramics at different temperatures: (a) the real part; (b) the imaginary part; and (c) tangent loss.

According to above analysis about phase evolution and solid-phase reaction, the separated amorphous free carbon had no contribution to the complex permittivity of SiBCN ceramics after annealing at 1400–1600 °C. However, the products of solid-phase reaction after annealing at 1700 °C, SiC, had a strong dissipation capacity to EMW. SiC can become the dipole and the dipole will steer under the electric field and arrange regularly in the field direction. The dipolar polarization will take a long relaxation time and attenuate much energy. Moreover, the interface charge polarization between SiC and the amorphous phase also need long relaxation times, which can reduce the EMW energy effectively.

As an important parameter for exhibiting the absorption properties of SiBCN ceramics, the reflection coefficient (*RC*) can be calculated according to the transmission line theory as follows, based on the metal back-panel model [32,33]:

$$RC(\text{dB}) = 20 \log \left| \frac{Z_{\text{in}} - 1}{Z_{\text{in}} + 1} \right| \quad (3)$$

where the normalized input impedance (Z_{in}) is given by the formula:

$$Z_{\text{in}} = \sqrt{\frac{\mu_r}{\varepsilon_r}} \tanh \left[j \left(\frac{2\pi f d}{c} \right) \sqrt{\mu_r \varepsilon_r} \right] \quad (4)$$

where $\varepsilon_r = \varepsilon' - j\varepsilon''$, $\mu_r = \mu' - j\mu''$, f is the EMW frequency (Hz), d is the thickness of the absorber (m), and c is the velocity of light in free space (m/s). Herein, μ_r is taken as 1 because of the negligible magnetic properties of the SiBCN ceramics. *RC* of SiBCN-Si₃N₄ ceramics heat-treated by different

temperatures with different sample thicknesses in the frequency range of 8.2–12.4 GHz are shown in Figure 7.

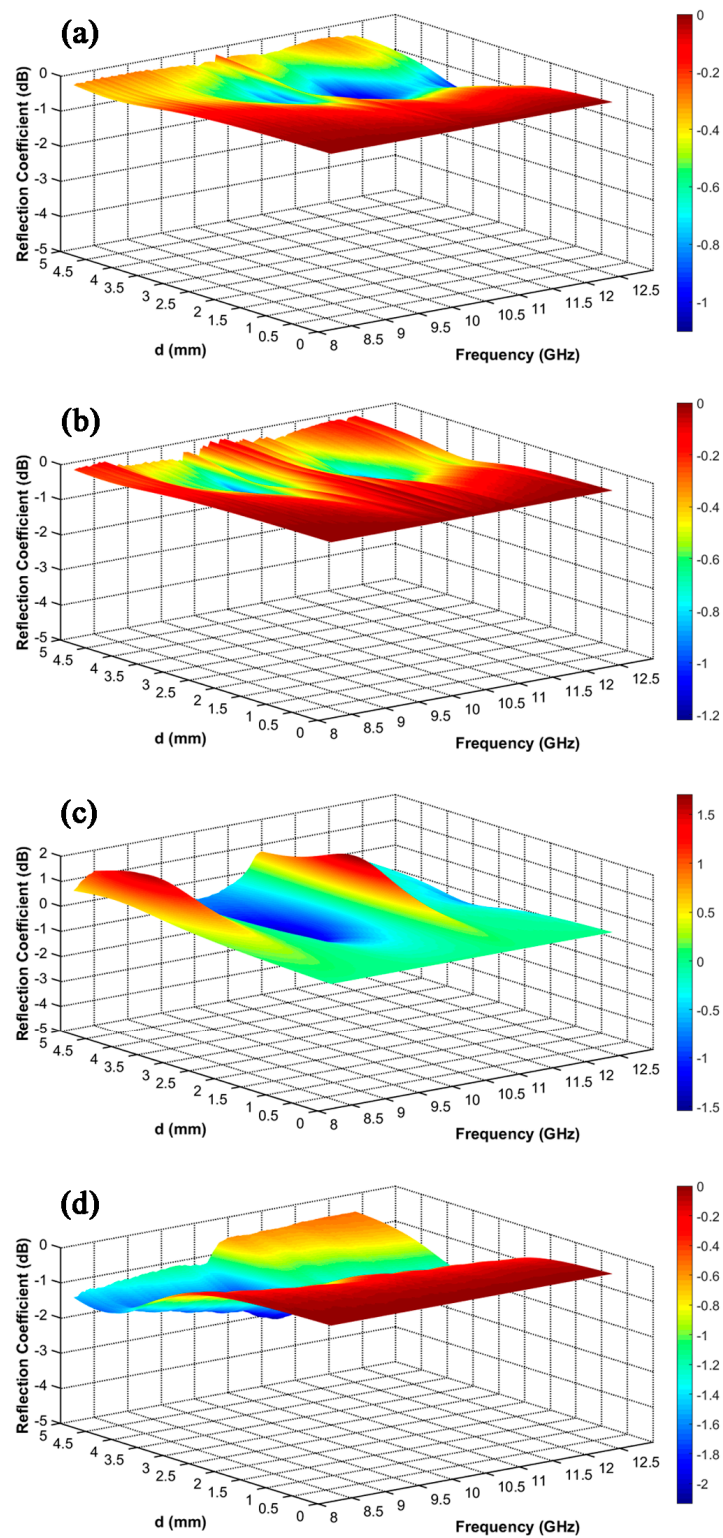


Figure 7. Reflection coefficient of SiBCN-Si₃N₄ ceramics heat-treated by different temperatures with different sample thicknesses in the frequency range of 8.2–12.4 GHz: (a) HT-14; (b) HT-15; (c) HT-16; and (d) HT-17.

SiBCN-Si₃N₄ ceramics showed higher RC after annealing from 1400 to 1700 °C, with a minimum RC of ca. −2 dB. Although the imaginary part of the permittivity of SiBCN-Si₃N₄ increased after annealing at 1700 °C, it was still at a low level. That is why RC of SiBCN-Si₃N₄ ceramics stayed so high. RC of SiBCN ceramics [16] fabricated by pyrolysis of liquid polyborosilazane gradually decreased with the annealing temperature increasing, and reached −15.78 dB at a thickness of 2.31 mm when annealed at 1650 °C. In our previous study of SiBCN ceramics deposited at 900 °C [24], SiBCN-Si₃N₄ ceramics with a dielectric loss of 0.1 showed proper dielectric properties. We want to study whether SiBCN ceramics deposited at lower temperature can also attain a better dielectric property after heat treatment. However, amounts of SiBCN introduced in SiBCN-Si₃N₄ at 800 °C was small and the free carbon was consumed after annealing at 1700 °C. Additionally, the amount of SiC formed was very small. All led to the lower EMW absorption property of the final SiBCN-Si₃N₄ composite ceramics.

Compared with the as-fabricated SiBCN ceramics, the ceramics annealed at 1700 °C can obtain different dielectric property, which can be attributed to the generation of SiC by phase-reaction. This work helped to further understand the microstructures of SiBCN ceramics. Since the element content and phase composition of SiBCN can be optimized by controlling the deposition parameters, including the ratios of precursor gases, the loss phase SiC can be separated by annealing at high temperature.

4. Conclusions

SiBCN-Si₃N₄ composite ceramics fabricated by introducing SiBCN into porous Si₃N₄ substrates were annealed at 1400–1700 °C. Amorphous free carbon, BN, and α-Si₃N₄ began to be separated at 1400 °C and 1600 °C, respectively. β-SiC began to be separated at 1500 °C. When the temperature increased to 1700 °C, more β-SiC formed by the reaction between free carbon and α-Si₃N₄. Consequently, the dielectric loss of composite ceramics increased to 0.03 from 0 due to the uniformly distributed SiC grains and the grain boundary.

Acknowledgments: This work was supported by the Chinese National Foundation for Natural Sciences under Contracts (no. 51472201, 51672217, 51602258), Shaanxi International Cooperation and Exchange of Scientific Projects (no. 2015KW-015), International S and T Cooperation Program of China (ISTCP no. 2014DFA50240), the State Key Laboratory of Advanced Refractories (201501), and the Research Fund of the State Key Laboratory of Solidification Processing (grant no. 120-TZ-2015).

Author Contributions: Jianping Li and Yongsheng Liu conceived and designed the experiments; Mingxi Zhao and Nan Chai performed the experiments; Jianping Li, Fang Ye and Hailong Qin analyzed the data; Laifei Cheng and Litong Zhang contributed reagents/materials/experiments/analysis tools; and Jianping Li wrote the paper.

Conflicts of Interest: The authors declare no conflict of interest. The founding sponsors had no role in the design of the study; in the collection, analyses, or interpretation of data; in the writing of the manuscript, and in the decision to publish the results.

References

1. Lee, S.H.; Weinmann, M.; Aldinger, F. Processing and properties of C/Si-B-C-N fiber-reinforced ceramic matrix composites prepared by precursor impregnation and pyrolysis. *Acta Mater.* **2008**, *56*, 1529–1538. [[CrossRef](#)]
2. Lee, S.-H.; Weinmann, M.; Gerstel, P.; Aldinger, F. Extraordinary thermal stability of sic particulate-reinforced polymer-derived Si-B-C-N composites. *Scr. Mater.* **2008**, *59*, 607–610. [[CrossRef](#)]
3. Lee, S.H.; Weinmann, M. C fiber/SiC filler/Si-B-C-N matrix composites with extremely high thermal stability. *Acta Mater.* **2009**, *57*, 4374–4381. [[CrossRef](#)]
4. Li, D.X.; Yang, Z.H.; Jia, D.C.; Duan, X.M.; He, P.G.; Zhou, Y. Ablation behavior of graphene reinforced sibcn ceramics in an oxyacetylene combustion flame. *Corros. Sci.* **2015**, *100*, 85–100. [[CrossRef](#)]
5. Wang, J.Y.; Yang, Z.H.; Duan, X.M.; Jia, D.C.; Zhou, Y. Microstructure and mechanical properties of sicf/sibcn ceramic matrix composites. *J. Adv. Ceram.* **2015**, *4*, 31–38. [[CrossRef](#)]
6. Ye, F.; Zhang, L.T.; Yin, X.W.; Zhang, Y.J.; Kong, L.; Liu, Y.S.; Cheng, L.F. Dielectric and microwave-absorption properties of sic nanoparticle/sibcn composite ceramics. *J. Eur. Ceram. Soc.* **2014**, *34*, 205–215. [[CrossRef](#)]

7. Riedel, R.; Kienzle, A.; Dressler, W.; Ruwisch, L.; Bill, J.; Aldinger, F. A silicoboron carbonitride ceramic stable to 2000 °C. *Nature* **1996**, *382*, 796–798. [[CrossRef](#)]
8. Weinmann, M.; Schuhmacher, J.; Kummer, H.; Prinz, S.; Peng, J.; Seifert, H.J.; Christ, M.; Müller, K.; Bill, J.; Aldinger, F. Synthesis and thermal behavior of novel Si-BCN ceramic precursors. *Chem. Mater.* **2000**, *12*, 623–632. [[CrossRef](#)]
9. Zhang, P.F.; Jia, D.C.; Yang, Z.H.; Duan, X.M.; Zhou, Y. Progress of a novel non-oxide Si-B-C-N ceramic and its matrix composites. *J. Adv. Ceram.* **2012**, *1*, 157–178. [[CrossRef](#)]
10. Han, M.; Yin, X.; Duan, W.; Ren, S.; Zhang, L.; Cheng, L. Hierarchical graphene/sic nanowire networks in polymer-derived ceramics with enhanced electromagnetic wave absorbing capability. *J. Eur. Ceram. Soc.* **2016**, *36*, 2695–2703. [[CrossRef](#)]
11. Duan, W.; Yin, X.; Ye, F.; Li, Q.; Han, M.; Liu, X.; Cai, Y. Synthesis and emw absorbing properties of nano sic modified PDC-SiOC. *J. Mater. Chem. C* **2016**, *4*, 5962–5969. [[CrossRef](#)]
12. Melvin, G.J.H.; Ni, Q.-Q.; Wang, Z. Performance of barium titanate@carbon nanotube nanocomposite as an electromagnetic wave absorber. *Phys. Status Solidi A* **2017**, *214*. [[CrossRef](#)]
13. Huo, J.; Wang, L.; Yu, H. Polymeric nanocomposites for electromagnetic wave absorption. *J. Mater. Sci.* **2009**, *44*, 3917–3927. [[CrossRef](#)]
14. Melvin, G.J.H.; Ni, Q.-Q.; Suzuki, Y.; Natsuki, T. Microwave-absorbing properties of silver nanoparticle/carbon nanotube hybrid nanocomposites. *J. Mater. Sci.* **2014**, *49*, 5199–5207. [[CrossRef](#)]
15. Li, Q.; Yin, X.; Duan, W.; Kong, L.; Hao, B.; Ye, F. Electrical, dielectric and microwave-absorption properties of polymer derived sic ceramics in x band. *J. Alloys Compd.* **2013**, *565*, 66–72. [[CrossRef](#)]
16. Ye, F.; Zhang, L.T.; Yin, X.W.; Zhang, Y.J.; Kong, L.; Li, Q.; Liu, Y.S.; Cheng, L.F. Dielectric and emw absorbing properties of PDCs- SiBCN annealed at different temperatures. *J. Eur. Ceram. Soc.* **2013**, *33*, 1469–1477. [[CrossRef](#)]
17. Sun, X.; Liu, H.T.; Li, J.S.; Cheng, H.F. Effects of CVD SiBCN interphases on mechanical and dielectric properties of Sic F/Sic composites fabricated via a pip process. *Ceram. Int.* **2016**, *42*, 82–89. [[CrossRef](#)]
18. Riedel, R.; Mera, G.; Hauser, R.; Klonczynski, A. Silicon-based polymer-derived ceramics: Synthesis properties and applications—A review. *J. Ceram. Soc. Jpn.* **2006**, *114*, 425–444. [[CrossRef](#)]
19. Wilden, J.; Wank, A.; Bykava, A. Dc thermal plasma CVD synthesis of coatings from liquid single source sibcn and sicuti precursors. *Surf. Coat. Technol.* **2005**, *200*, 612–615. [[CrossRef](#)]
20. Dong, N.; Chai, N.; Liu, Y.; Liu, X.; Qin, H.; Zhang, X.Y.L.; Cheng, L. Thermodynamic analysis on deposition of Si B C N ceramic by low pressure chemical vapor deposition/infiltration from SiCH₃Cl₃-BCl₃-NH₃-H₂-Ar system. *J. Eur. Ceram. Soc.* **2016**, *36*, 3581–3591. [[CrossRef](#)]
21. Vlcek, J.; Potocky, S.; Cizek, J.; Houska, J.; Kormunda, M.; Zeman, P.; Perina, V.; Zemek, J.; Setsuhara, Y.; Konuma, S. Reactive magnetron sputtering of hard Si-B-C-N films with a high-temperature oxidation resistance. *J. Vac. Sci. Technol. A* **2005**, *23*, 1513–1522. [[CrossRef](#)]
22. Yang, Z.-H.; Jia, D.-C.; Zhou, Y.; Yu, C.-Q. Fabrication and characterization of amorphous SiBCN powders. *Ceram. Int.* **2007**, *33*, 1573–1577. [[CrossRef](#)]
23. Wang, Z.-C.; Aldinger, F.; Riedel, R. Novel silicon-boron-carbon nitrogen materials thermally stable up to 2200 °C. *J. Am. Ceram. Soc.* **2001**, *84*, 2179–2183. [[CrossRef](#)]
24. Liu, Y.S.; Chai, N.; Liu, X.F.; Qin, H.L.; Yin, X.W.; Zhang, L.T.; Cheng, L.F. The microstructure and dielectric properties of SiBCN ceramics fabricated via LPCVD/CVI. *J. Am. Ceram. Soc.* **2015**, *98*, 2703–2706. [[CrossRef](#)]
25. Xue, J.; Yin, X.; Pan, H.; Liu, X.; Zhang, L.; Cheng, L. Crystallization mechanism of CVD Si₃N₄-SiCN composite ceramics annealed in N₂ atmosphere and their excellent emw absorption properties. *J. Am. Ceram. Soc.* **2016**, *99*, 2672–2679. [[CrossRef](#)]
26. Yin, X.W.; Li, X.M.; Zhang, L.T.; Cheng, L.F.; Liu, Y.S.; Pan, T.H. Microstructure and mechanical properties of Lu₂O₃-doped porous silicon nitride ceramics using phenolic resin as pore-forming agent. *Int. J. Appl. Ceram. Technol.* **2010**, *7*, 391–398. [[CrossRef](#)]
27. Mera, G.; Riedel, R.; Poli, F.; Müller, K. Carbon-rich SiCN ceramics derived from phenyl-containing poly(silylcarbodiimides). *J. Eur. Ceram. Soc.* **2009**, *29*, 2873–2883. [[CrossRef](#)]
28. Ferrari, A.C.; Robertson, J. Interpretation of raman spectra of disordered and amorphous carbon. *Phys. Rev. B* **2000**, *61*, 14095–14107. [[CrossRef](#)]

29. Tsutsui, H.; Matsutani, T.; Kawasaki, T. Development of B-C-N-O diaphragm for environmental cell transmission electron microscope by plasma enhanced chemical vapor deposition. *AIP Conf. Proc.* **2010**, *1282*, 39–43.
30. Jedrzejowski, P.; Cizek, J.; Amassian, A.; Klemberg-Sapieha, J.E.; Vlcek, J.; Martinu, L. Mechanical and optical properties of hard SiCN coatings prepared by pecvd. *Thin Solid Films* **2004**, *447–448*, 201–207. [[CrossRef](#)]
31. Jeon, J.-H.; Choi, S.R.; Chung, W.S.; Kim, K.H. Synthesis and characterization of quaternary Ti-Si-C-N coatings prepared by a hybrid deposition technique. *Surf. Coat. Technol.* **2004**, *188–189*, 415–419. [[CrossRef](#)]
32. Melvin, G.J.H.; Ni, Q.-Q.; Natsuki, T.; Wang, Z.; Morimoto, S.; Fujishige, M.; Takeuchi, K.; Hashimoto, Y.; Endo, M. Ag/CNT nanocomposites and their single- and double-layer electromagnetic wave absorption properties. *Synth. Met.* **2015**, *209*, 383–388. [[CrossRef](#)]
33. Ni, Q.-Q.; Melvin, G.J.H.; Natsuki, T. Double-layer electromagnetic wave absorber based on barium titanate/carbon nanotube nanocomposites. *Ceram. Int.* **2015**, *41*, 9885–9892. [[CrossRef](#)]



© 2017 by the authors. Licensee MDPI, Basel, Switzerland. This article is an open access article distributed under the terms and conditions of the Creative Commons Attribution (CC BY) license (<http://creativecommons.org/licenses/by/4.0/>).